Featured in Physics

Dissipative Stabilization of Squeezing Beyond 3 dB in a Microwave Mode

R. Dassonneville,[1] R. Assouly,[1] T. Peronnin,[1] A.A. Clerk,[2] A. Bienfait,[1] and B. Huard[1,*]

[1] *University of Lyon, ENS de Lyon, University Claude Bernard, CNRS, Laboratoire de Physique, Lyon F-69342, France*

[2] *Pritzker School of Molecular Engineering, University of Chicago, Chicago, Illinois 60637, USA*

(Received 4 February 2021; accepted 15 April 2021; published 20 May 2021)

While a propagating state of light can be generated with arbitrary squeezing by pumping a parametric resonator, the intraresonator state is limited to 3 dB of squeezing. Here, we implement a reservoir-engineering method to surpass this limit using superconducting circuits. Two-tone pumping of a three-wave-mixing element implements an effective coupling to a squeezed bath, which stabilizes a squeezed state inside the resonator. Using an ancillary superconducting qubit as a probe allows us to perform a direct Wigner tomography of the intraresonator state. The raw measurement provides a lower bound on the squeezing at about 6.7 ± 0.2 dB below the zero-point level. Further, we show how to correct for resonator evolution during the Wigner tomography and obtain a squeezing as high as 8.2 ± 0.8 dB. Moreover, this level of squeezing is achieved with a purity of 0.91 ± 0.09.

DOI: 10.1103/PRXQuantum.2.020323

I. INTRODUCTION

One of the most striking predictions of quantum mechanics is that even in the ground state of an harmonic oscillator, any quadrature measurement is noisy. Zero-point fluctuations can however be engineered and lowered for one quadrature of the field at the expense of the other. These squeezed states have become a central resource for quantum information processing. It is thus desirable to maximize their squeezing factor, expressed as the reduction ratio of the variance of the squeezed quadrature. Squeezed states can be used to boost the sensitivity of many measurements including gravitational-wave detection [1–4], perform quantum secure communication [5,6], and used for measurement-based continuous-variable quantum computing [6,7].

While most applications could deal with transient squeezing by timing the control sequences properly, an ideal resource consists in generating a steady squeezed state. Steady-state squeezing can occur in stationary or propagating modes. For the latter, it is typically achieved by parametrically pumping a resonator coupled to a single port. This process generates quadrature squeezing of the outgoing field but also of the intraresonator field. Both quantities are related by the input-output relation stating that the intraresonator field is the superposition of the incoming field and the outgoing field [8]. While any amount of squeezing can theoretically be obtained for the outgoing field, this superposition imposes that the steady-state intraresonator quadrature variance is limited to 1/2 of the vacuum fluctuations, which is the average between the variance of the incoming field (vacuum fluctuations) and the arbitrarily low variance of the outgoing field. This is the so-called 3-dB limit [9,10].

Intraresonator steady-state squeezing beyond 3 dB can, in principle, be attained by injecting squeezed light into the resonator input using an external source of squeezed radiation [11–16]. In practice however, the achievable squeezing in such schemes is limited by losses associated with transporting and injecting the extremely fragile squeezed state into the resonator. A more attractive approach is to use reservoir-engineering techniques [17], where tailored driving results in the cavity being coupled to effective squeezed dissipation [18–20]. These methods can also surpass the 3-dB limit, and do not involve transporting an externally prepared squeezed state. Reservoir-engineering intracavity squeezing beyond 3 dB has recently been achieved for mechanical modes, both in optomechanical systems [21–24] as well as in a trapped ion platform [25].

In this work, we experimentally demonstrate that reservoir-engineering squeezing can also be achieved for purely electromagnetic intracavity modes, namely a microwave-frequency mode in a superconducting quantum circuit. Using the well-developed circuit-QED toolbox, we also perform a direct tomography of the intraresonator

*benjamin.huard@ens-lyon.fr

squeezed state instead of inferring the resonator state from the measured output mode. This is achieved through the use of an ancillary superconducting qubit, which enables *in situ* Wigner tomography of the squeezed intracavity microwave mode. The intracavity squeezing factor reaches at least -6.7 ± 0.2 dB, going well beyond the 3-dB limit. We also probe the nonclassicality of the squeezed state by investigating its photon-number statistics [13], and use our tomographic method to carefully study the full dynamics of the dissipative generation of squeezing. This work thus presents an interesting platform to stabilize, manipulate, and characterize Gaussian states *in situ*. Our stabilization technique could also be extended beyond simple squeezed states to other continuous variable states such as cat or grid states [26–31] by taking advantage of the large nonlinearities that can be engineered in circuit-QED.

II. SYSTEM AND MODEL

Our device consists in a Josephson ring modulator [35] coupling one mode (the *cavity*), which we would like to stabilize in a squeezed state, and a second auxiliary mode strongly coupled to a transmission line (the *dump*). The cavity and dump have resonant frequencies $\omega_c/2\pi = 3.741\,55$ GHz and $\omega_d/2\pi = 11.382$ GHz and decay rates $\kappa_c/2\pi = 40$ kHz and $\kappa_d/2\pi = 8$ MHz. Our setup also has an ancillary transmon qubit coupled to the cavity; its only role is to perform intraresonator Wigner tomography [Fig. 1(a)].

When applying a pump at frequency $\omega_- = \omega_d - \omega_c$, and within the rotating-wave approximation (RWA) and stiff pump condition, the JRM leads to a beam-splitter interaction Hamiltonian $\hat{H}_-/\hbar = g_-\hat{d}^\dagger\hat{c} + g_-^*\hat{d}\hat{c}^\dagger$, where the pump amplitude controls the coupling strength g_- between the cavity and dump modes described by bosonic operators $\hat{c}$ and $\hat{d}$. It mediates coherent exchange of photons between the cavity and the dump and thus lossless frequency conversion [36,37]. In contrast, a pump applied at frequency $\omega_+ = \omega_d + \omega_c$ mediates a parametric down-conversion process involving cavity and dump, $\hat{H}_+/\hbar = g_+\hat{d}^\dagger\hat{c}^\dagger + g_+^*\hat{d}\hat{c}$. The pump amplitude controls the coupling strength g_+. On its own, this kind of pumping leads to phase-preserving amplification [35,38] and generation of two-mode squeezed states [39]. Note that in order to avoid parasitic nonlinear effects, we operate the JRM at a flux point, which maximizes these three-wave mixing terms while canceling the four-wave mixing terms [40,41].

Simultaneously pumping at these two frequencies enables various interesting phenomena such as effective ultrastrong coupling [42,43], injection and parametric locking [44], or directional amplification [45–47]. Here, using a long-lived cavity mode, we show that this double pumping scheme can stabilize a squeezed state [18,19]. Indeed, in the rotating frame, and setting the phase

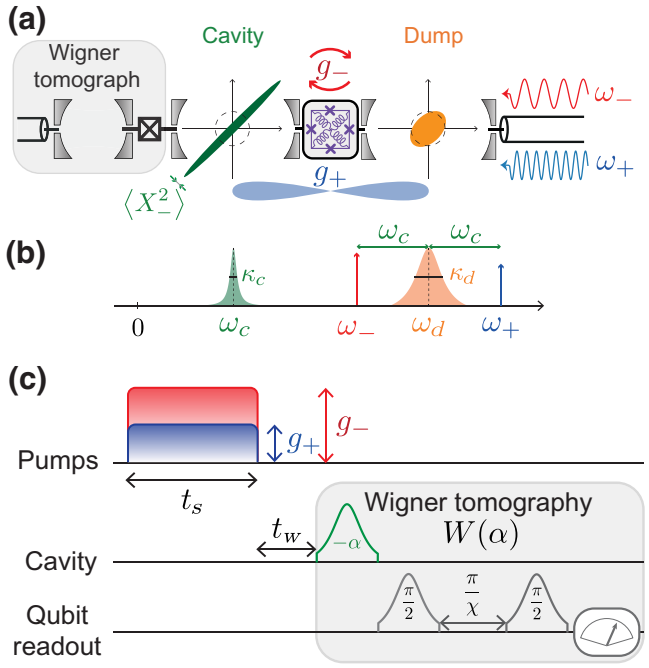

FIG. 1. (a) Principle of the experiment. A cavity mode (green) at frequency ω_c is coupled to a dump mode at frequency ω_d (orange) via a Josephson ring modulator (JRM, in purple). The dump mode is strongly coupled to a cold transmission line through which the JRM is pumped at both frequencies $\omega_+ = \omega_c + \omega_d$ (two-mode squeezing) and $\omega_- = \omega_d - \omega_c$ (photon conversion). A squeezed vacuum state is stabilized into the cavity as a result. An ancillary qubit with an ancillary readout resonator is used as a Wigner tomograph. The contours of the Wigner functions of each mode are shown as colored regions in the quadrature phase space, while a dashed circle represents the vacuum state. (b) Frequencies of the involved modes and drives. (c) Pulse sequence. The sum pump at ω_+ with amplitude g_+ and the difference pump at ω_- with amplitude g_- are applied for a time t_s. After a waiting time t_w, the Wigner function of the cavity $W(\alpha)$ is measured using a cavity displacement by $-\alpha$ followed by a parity measurement [32–34].

references such that $g_\pm$ are positive, the total Hamiltonian reads

$$\hat{H}/\hbar = \hat{d}(g_+\hat{c} + g_-\hat{c}^\dagger) + \text{h.c.} \tag{1}$$

By rewriting this Hamiltonian using a Bogoliubov transformation, we can show that the dump mode $\hat{d}$ is coupled to an effective mode $\hat{\beta} = \cosh(r)\hat{c} + \sinh(r)\hat{c}^\dagger$ with $r = \tanh^{-1}(g_+/g_-)$ when $g_+ < g_-$. This Bogoliubov mode $\hat{\beta}$ can be expressed as the transformation of mode $\hat{c}$ by the squeezing operator $\hat{S}(r) = \exp(r^*\hat{c}^2/2 - r\hat{c}^{\dagger 2}/2)$, $\hat{\beta} = \hat{S}(r)\hat{c}\hat{S}^\dagger(r)$. Placing mode β in its ground state corresponds to generating a squeezed vacuum state in the cavity mode $\hat{c}$. The strongly dissipative dump mode $\hat{d}$ can be used

for that purpose since it is directly coupled to $\hat{\beta}$ through

$$\hat{H}/\hbar = \mathcal{G}\hat{d}\hat{\beta}^\dagger + \text{h.c.}, \tag{2}$$

where the coupling strength reads $\mathcal{G} = \sqrt{g_-^2 - g_+^2}$. In the ideal case where the coupling rate κ_d of the dump mode to a reservoir at zero temperature is much larger than any other rates, and where the cavity lifetime κ_c^{-1} is unlimited, the Hamiltonian leads to the full relaxation of the Bogoliubov mode into its ground state and thus the cavity into a squeezed state.

The signature of this squeezing is best seen in the quadrature phase space of the cavity mode. We denote X_- and X_+ the quadratures of the cavity mode that have the smallest and largest variances in a given state. In the vacuum state of the cavity ($r = 0$), the variance of the quadratures corresponds to the zero-point fluctuations $\langle X_\pm^2\rangle_{|0\rangle} = X_0^2$. The squeezing factor one can generate in the ground state of the Bogoliubov mode is simply a scaling of the variances by the factor $S_\pm = \langle X_\pm^2\rangle/X_0^2 = e^{\pm 2r}$. In the general case, where the Bogoliubov mode is not cooled down to its ground state, these factors become [19]

$$S_\pm = e^{\pm 2r}\langle(\beta \mp \beta^\dagger)^2\rangle. \tag{3}$$

We thus see that in principle, the 3-dB squeezing limit can be surpassed arbitrarily by having g_+ approach g_- from below (as this causes the squeezing parameter r to diverge). The key ingredient breaking through the 3-dB limit is the re-engineering of the dissipation operator from $\hat{c}$ to its squeezed counterpart $\hat{\beta}$. In practice, squeezing is still limited because in this limit $g_+ \to g_-$ the effective coupling rate $\mathcal{G}$ of the Bogoliubov mode to the dump goes down to zero. As a result, the competition between this engineered decay channel and the intrinsic cavity loss (rate κ_c) prevents the Bogoliubov mode from reaching its ground state. This both degrades the effective squeezing of the steady state, as well as its purity. Thus, for any value of g_- there exists an optimum value of g_+ that minimizes the variance $\langle X_-^2\rangle$. This minimum increases with the value of g_- and is finally expected to saturate to a level set by the damping rates $S_- \geq \kappa_c/(\kappa_c + \kappa_d)$, which reflects the fact that the damping rate of the dump κ_d sets an upper limit to the coupling of the bosonic mode to the effective squeezed reservoir.

We thus see that a prerequisite for achieving squeezing well beyond 3 dB is to engineer a large ratio κ_d/κ_c. For our sample parameters, we have $\kappa_d \simeq 200\kappa_c$, leading to a lower bound of $S_- \geq -23$ dB [19]. Further, taking into account the thermal equilibrium occupancies n_c^{th} and n_d^{th} of the cavity and dump modes, and in the limit of the experiment where $\kappa_c, \mathcal{G} \ll \kappa_d$, Eq. (3) leads to (see Appendix C or Ref. [24] for the formula without approximation)

$$S_\pm \simeq \frac{\kappa_c(2n_c^{\text{th}} + 1) + \Gamma_\pm(2n_d^{\text{th}} + 1)}{\kappa_{\text{eff}}}, \tag{4}$$

where we introduce $\kappa_{\text{eff}} = \kappa_c + 4\mathcal{G}^2/\kappa_d$ and $\Gamma_\pm = 4(g_- \pm g_+)^2/\kappa_d$. Equation (4) also makes it clear that the intrinsic loss rate κ_c and nonzero environmental temperatures also lower the purity of the steady state $\mathcal{P} = \text{Tr}(\rho^2)$ below 1, where ρ is the steady-state cavity density matrix. This follows from the fact that $\mathcal{P} = 1/\sqrt{S_-S_+}$ for a Gaussian state.

To measure the squeezing and antisqueezing factors $S_\pm$, we perform a full *in situ* Wigner tomography [32–34] using an ancillary transmon qubit at frequency $\omega_q/2\pi = 4.327\,31$ GHz [Fig. 1(a)]. It couples dispersively to the cavity with a dispersive shift $\chi/2\pi = -3.28$ MHz. A third resonator, at frequency $\omega_r/2\pi = 6.293$ GHz, is used to perform single-shot readout of the qubit state with a fidelity of 96% in a 380-ns integration time. Another option to infer the quantum state inside of the cavity is to probe the quantum state of the output dump mode that should be a squeezed state [24,43,48]. Thus, this two-tone pumping scheme can also be used to generate propagating squeezed state [49,50]. From the Wigner function, we compute the covariance matrix of the cavity-mode quadratures and diagonalize it to extract the minimum and maximum cavity quadrature variances $\langle X_\pm^2\rangle$. Due to its coupling to the qubit, the cavity acquires an induced parasitic self-Kerr nonlinearity $-K\hat{c}^{\dagger 2}\hat{c}^2$ and a qubit-state-dependent self-Kerr $-K_e\hat{c}^{\dagger 2}\hat{c}^2|e\rangle\langle e|$ with $K/2\pi = 20$ kHz and $K_e/2\pi = 70$ kHz (measured in a previous run of the experiment). These nonlinearities distort the squeezed state and thus reduce the effective squeezing factor, similarly to what occurs for Josephson parametric amplifiers (JPAs) [51]. While no analytical solution taking into account the Kerr effects exists, Eqs. (3) and (4) still provide a good description when $\mathcal{G} \gg K$. In the future, these nonlinearities could be harnessed as a resource to stabilize more complex non-Gaussian states [26,27,52,53].

III. STEADY-STATE SQUEEZING

The key advantage of reservoir engineering is that the desired target state is prepared in the steady state, independent of the initial cavity state: one can simply turn on the pumps and wait. We thus turn on g_+ and g_- for a duration $t_s = 4\ \mu$s [cf. Fig. 1(c)] that is long enough to establish a steady state, and immediately afterwards measure the Wigner function $W(\alpha)$. To perform the measurement at each amplitude α, we start by applying a calibrated displacement $D(-\alpha)$ to the cavity state using a cavity drive at ω_c with a pulse shape chosen to be a 13-ns-wide hyperbolic secant and whose complex amplitude is proportional to $-\alpha$. We then measure the cavity parity operator by reading

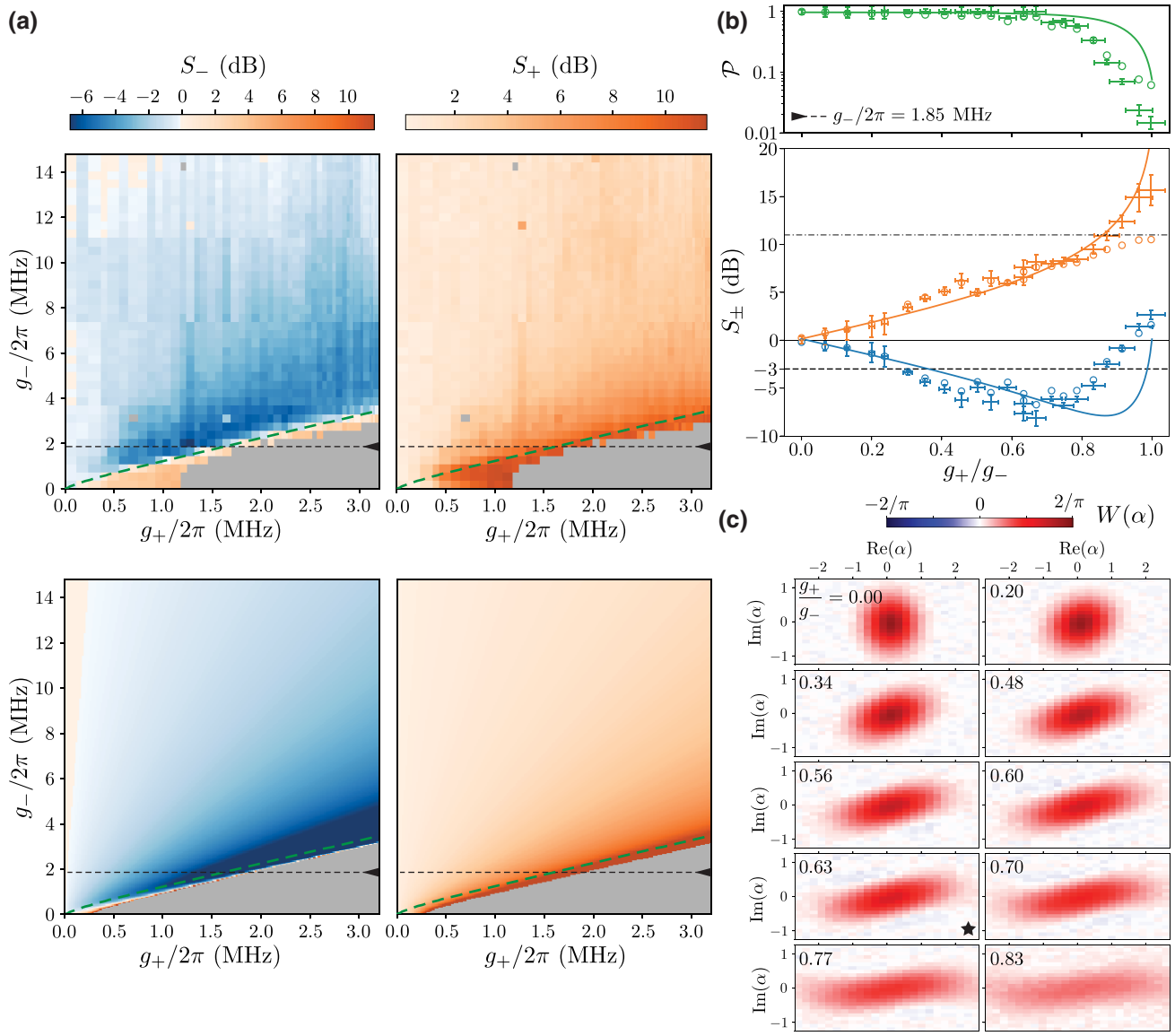

FIG. 2. Characterization of the stabilized squeezed state. (a) Top panels: measured steady-state squeezing $S_- = \langle X_-^2\rangle/X_0^2$ (left) and antisqueezing $S_+ = \langle X_+^2\rangle/X_0^2$ (right) factors. Bottom panels: theoretical prediction for $S_\pm$ using Eq. (4). Green dashed lines correspond to the value g_-^{opt} as a function of g_+ that minimizes the squeezing S_- according to Eq. (4) (i.e., calculated by neglecting Kerr nonlinearities). (b) Purity $\mathcal{P}$ (top, green), squeezing S_- (bottom, blue) and antisqueezing S_+ (bottom, orange) factors as a function of g_+/g_- for a fixed value $g_-/2\pi = 1.85$ MHz [cut along the arrow in (a)]. Circles are the normalized eigenvalues of the covariance matrix of the measured Wigner functions at each pump amplitude as shown in (c) and reach a squeezing factor as low as $S_- = -6.7 \pm 0.2$ dB. Points with error bars are the values obtained when correcting for cavity evolution during Wigner tomography (see Appendix D 1), which reveals a stabilized squeezing reaching as low as $S_- = -8.2 \pm 0.8$ dB. Solid lines come from the model Eq. (4). (c) Selected measured Wigner functions along the same axis $g_-/2\pi = 1.85$ MHz, for various g_+/g_- ratios as indicated in the labels. The star indicates the Wigner function at optimum squeezing.

out the qubit state after performing two $\pi/2$ unconditional pulses on the qubit separated by a waiting time $\pi/\chi = 152$ ns. We perform phase-cycling, running each sequence twice with an opposite phase for the second $\pi/2$ pulse, so as to remove most of the parasitic contribution of higher-order Kerr effects [54]. The Wigner function is probed on a discretized phase space using a rectangular grid of 25×25 pixels approximately aligned to the squeezing axis. Due to the finite window size (cf. Appendix E), we could resolve only antisqueezing up to 11 dB [dotted dash line in Fig. 2(b)]. Each Wigner tomogram is averaged over 5000 realizations. To increase the repetition rate and limit the low-frequency drifts, the cavity is first emptied by applying a difference pump g_-, cooling it down to a thermal vacuum

state with residual population $n_c^{\rm th} = n_d^{\rm th} = 0.017 \pm 0.003$ (see Appendix B 3). The qubit is also reset to its ground state using measurement-based feedback. Furthermore, to minimize the low-frequency noise as much as possible, we interleave pump-on measurements with pump-off measurements. We thus obtain experimental squeezing factors $S_\pm = \left(\langle X_\pm^2\rangle / \langle X^2\rangle_{\rm off}\right) \times \left(\langle X^2\rangle_{\rm off}/X_0^2\right)$ by first normalizing the measured variances $\langle X_\pm^2\rangle$ with the measured pump-off variances $\langle X^2\rangle_{\rm off}$ and then correcting for the thermal occupancy $\langle X^2\rangle_{\rm off}/X_0^2 = 0.15 \pm 0.03$ dB. The pumping strengths g_+ and g_- are calibrated using independent measurements (Appendix B 1). We estimate a statistical uncertainty of ± 0.2 dB on the variances extracted from the measured Wigner functions.

The obtained steady-state squeezing and antisqueezing factors are displayed in Fig. 2(a) as a function of g_+ and g_-. We observe a maximum squeezing of -6.7 ± 0.2 dB well below the -3-dB limit, which we believe to be the highest squeezing factor observed in an intracavity microwave mode. Correspondingly, we extract an antisqueezing of 7.7 ± 0.2 dB and thus a state purity of 0.89 ± 0.04. For each value of the rate g_+, the largest squeezing we observe occurs for g_- close to g_+. This trend is expected from the analytical Kerr-free model Eq. (4) of the system, which predicts the working point of largest squeezing as a function of g_+ [green dashed line in Fig. 2(a)] [19]. However, contrary to the expected monotonic increase of the optimal squeezing factor S_- with g_+ [Kerr-free prediction in the bottom panels of Fig. 2(a)], we find a global maximum squeezing at a finite value of (g_-, g_+). Note that for $g_+ > g_-$ the system becomes unstable: the qubit gets ionized [55], preventing us from measuring the Wigner functions (gray shade area).

In Figs. 2(b) and 2(c), we show the squeezing and antisqueezing as a function of g_+/g_- as well as some measured Wigner tomograms, for $g_-/2\pi = 1.85$ MHz. For $g_+ < 0.7 g_-$, the measured variances are well captured by Eq. (4) with exponentially increasing squeezing factors. For $g_+ > 0.7 g_-$, the measured variances start deviating from the theory [solid lines in Fig. 2(b)]. As can be seen in Fig. 2(c), the squeezed states are not Gaussian anymore in this parameter region. The Wigner functions develop an S shape, a typical signature of the cavity self-Kerr. We attribute this effect to the higher-order terms we neglect so far: the self-Kerr rate induced by the qubit on the cavity, as well as a residual four-wave mixing term in the JRM Hamiltonian (see Appendix D 2).

While the raw measurement of the Wigner function provides a good estimate of the steady-state squeezing parameter [circles in Fig. 2(b)], the finite measurement time needed to perform tomography leads to a systematic error. During this finite measurement time, the pump tones $g_\pm$ are off, implying that the cavity is no longer coupled to an effective squeezed reservoir. The squeezed state thus degrades due to the intrinsic cavity loss. A further error is caused by evolution under the cavity self-Kerr nonlinearity during this time. Both these effects cause our Wigner-function methods to *underestimate* the true value of the steady-state squeezing.

It is possible to correct for this measurement error and retropredict via numerical simulation the squeezing factors $S_\pm$ associated with the state prepared at the end of the stabilization period [56]. To that end, we consider a series of input model Gaussian states for which we numerically implement our experimental Wigner tomography measurement. At the end of these simulations, we obtain a mapping from Gaussian states to measured squeezing and antisqueezing factors that we are able to invert in order to retropredict the stabilized state (Appendix D 1). Using this correction improves the best squeezing estimate to -8.2 ± 0.8 dB [dots with error bars in Fig. 2(b)] with purity 0.91 ± 0.09.

It is interesting to compare our stabilization technique to other intraresonator microwave squeezing generation schemes. One possibility consists in driving a cavity with a squeezed input state that is externally generated by a Josephson parametric amplifier [11,12,15,16,57]. High squeezing factors [51,57–59] ($\simeq -10$ dB) can be achieved in the amplifier output field. However, transferring this state into a cavity is challenging as it is extremely sensitive to microwave losses, resulting in degraded squeezing and purity. For comparison, we consider a resonator driven by a pure squeezing source (in practice a JPA). To achieve the same intracavity squeezing and purity as our setup ($S_- = -8.2$ dB and $\mathcal{P} = 0.91$, respectively), the source would need to generate an output squeezing better than approximately -9.1 dB and the losses between the source and the resonator would need to be kept below 0.15 dB. This level of loss is smaller than the typical insertion loss of common microwave components. It is hard to achieve, even if all elements are fabricated in a single-chip architecture. We can also compare against another approach for generating (but not stabilizing) a squeezed state, based on the use of arbitrary state-preparation techniques (e.g., the SNAP gate protocol [60]). In Ref. [61], the authors used such an approach to obtain a squeezing factor of -5.71 dB for a purity of 0.82 with a nondeterministic success rate of 15%. We note that for trapped ions, modulating the resonance frequency at twice its natural frequency demonstrated transient squeezing as large as 17.2 dB [62,63].

IV. NONCLASSICAL PHOTON DISTRIBUTION

One of the hallmarks of vacuum squeezed states is that they are quantum superpositions involving only even-number photon Fock states. Such ideal states have the form $|\psi\rangle = \cosh(r)^{-1/2} \sum_{k=0}^{\infty} \tanh(r)^k [\sqrt{(2k)!}/2^k k!] |2k\rangle$. We could use the measured Wigner functions to compute the probability $\mathbb{P}(n)$ that the cavity contains n photons.

However for large n, the accuracy of this method is strongly hampered by the limited size of the measured quadrature phase space. Our device allows us to directly verify this unique, nonclassical aspect of the squeezed states we stabilize in our cavity [15]. This is because our coupling to the ancilla qubit is strong enough to place us in photon-number-resolved regime where distinct cavity photon numbers can be resolved by measuring the effective qubit frequency, i.e., $\chi \gg \Gamma_2$ with $\Gamma_2 = (11\ \mu\text{s})^{-1}$ the qubit coherence rate.

After preparing the squeezed state, we perform spectroscopy of the qubit using a narrow-bandwidth π pulse at a varying probe frequency ω followed by qubit readout

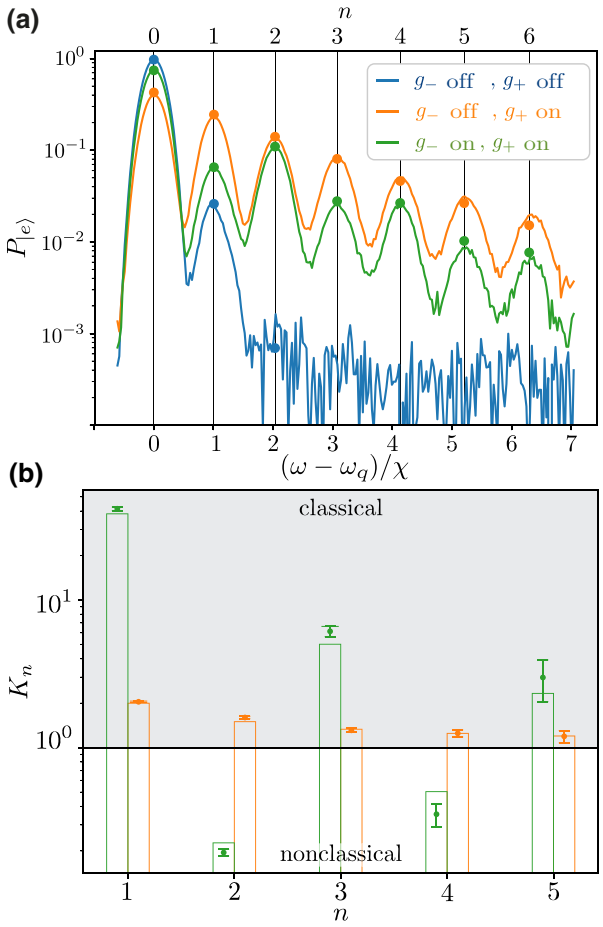

FIG. 3. (a) Number photon-distribution measurement using qubit spectroscopy. Solid lines: measured probability $P_{|e\rangle}$ that the qubit gets excited by a 200-ns-wide hyperbolic secant π pulse of frequency ω after a cavity state is stabilized. Blue: near vacuum state when no pumps are applied. Orange: thermal state when only a pump g_+ is applied. Green: squeezed vacuum state when both pumps g_+ and g_- are applied. Vertical lines indicate the qubit resonance frequency conditioned on the cavity having n photons. Filled circles: numerical simulations. (b) Dots with error bars: Klyshko number K_n (see main text) calculated from the qubit spectroscopy. Orange bars: expected Klyshko number for a thermal state at any temperature. Green bars: Klyshko numbers predicted with the model described in the text.

[green curve in Fig. 3(a)]. The observed peak heights at each frequency $\omega - \omega_q \approx n\chi$ allow us to determine the cavity photon-number distribution $\mathbb{P}(n)$ [64]. We correct this dataset for the qubit residual thermal population (1%), the finite fidelity of the π pulse and readout errors. Interestingly, the peaks are not evenly spaced in frequency due to the higher nonlinear term $-K_e\hat{c}^{\dagger 2}\hat{c}^2|e\rangle\langle e|$ with $K_e/2\pi = 70$ kHz. The photon-number distributions $\mathbb{P}(n)$ are then obtained from the qubit excitation probability at $\omega_q - n(\chi + 2K_e n)$ (vertical lines). For comparison, we also measure the photon-number distribution $\mathbb{P}(n)$ for two other cavity states: a thermal equilibrium state when no pumps are applied (blue in Fig. 3) and a thermal state that we create by only applying a sum pump $g_+/2\pi = 0.43$ MHz (orange curve). Note that this thermal state is obtained by tracing out the dump mode for the vacuum two-mode squeezed state that is stabilized between cavity and dump [65].

For the squeezed state (green curve with $g_-/2\pi = 2.2$ MHz, $g_+/2\pi = 1.42$ MHz), we observe a nonmonotonic behavior: the weight of even photon numbers is enhanced, whereas that of odd photon numbers is suppressed (note the log scale here). The nonzero but small population of odd Fock states indicates a deviation from an ideal squeezed vacuum state. The measured data closely fits to our numerical simulation [dots in Fig. 3(a)]. The measurement done with the pumps off (after emptying the cavity into the dump and resetting the qubit as above) gives the thermal population of the cavity $n_c^{\text{th}} = 0.017$ (blue dots) and also indicates the measurement noise floor. For the thermal state, we observe a Bose-Einstein distribution with a population $n_c^{\text{th}} = 1.5$ (orange dots).

Even though their Wigner function is always positive, squeezed states are typically regarded as nonclassical states as they cannot be represented as statistical mixtures of coherent states. Formally, this means that they do not have well-behaved Glauber-Sudarshan P representations [66]. Equivalently, it also manifests itself in the behavior of so-called Klyshko numbers $K_n = (n+1)\mathbb{P}(n-1)\mathbb{P}(n+1)/n\mathbb{P}(n)^2$. A state is nonclassical if for one or more integers n, $K_n < 1$ (as this implies that the P function cannot be well behaved). It can be shown that for an arbitrary squeezed state, this nonclassical criterion is reached for $S_- < 1$ [67]. For example, a perfect squeezed vacuum state, as it only includes even photon numbers, exhibits infinite odd Klyshko numbers and zero even Klyshko numbers. Ref. [15] computed the Klyshko numbers for a squeezed state generated by an external JPA and observed a Klyshko number smaller than 1, even though they only observed monotonic behavior in the photon distribution $\mathbb{P}(n)$.

For a thermal state, the Klyshko number is given by $K_n^{\text{th}} = (n+1)/n$ independently of temperature [orange bars in Fig. 3(b)]. We observe this universal relation with the prepared thermal state (orange points with errorbar).

Interestingly, it is a striking demonstration of the fact that a two-mode squeezed state generates a thermal distribution when tracing out one of the modes. It is expected from the maximally entangled state at a given average energy. We do not show the Klyshko numbers when the pumps are off because $\mathbb{P}(n)$ is below the noise floor.

For the squeezed state, we observe ample oscillations in the Klyshko numbers (notice the log scale again). We measure $K_2 = 0.23$ and $K_4 = 0.5$ that are well below one (green points with errorbars). Similarly to the cavity population $\mathbb{P}(n)$, our numerical model (green bars) reproduces the observed Klyshko numbers.

V. STABILIZATION DYNAMICS AND DECAY OF SQUEEZING

Our measurements establish that, as expected, the reservoir-engineering scheme we implement is able to stabilize a squeezed state in the cavity. In addition to characterizing the steady state, it is also interesting to ask how long the scheme takes to prepare the steady state. For the ideal (Kerr-free) system, and in the limit of a large dump-mode damping, one can use adiabatic elimination to show that this preparation timescale is $\kappa_d/\mathcal{G}^2$ [19].

We can directly test this prediction in our experiment. The measured squeezing and antisqueezing factors are shown in Fig. 4(a) as a function of the time t_s during which the pumps are turned on for $g_+/2\pi = 1.16$ MHz and for various values of g_-. By normalizing the squeezing and antisqueezing factors $S_\pm$ by their steady-state values $S_\pm^{\rm ss}$, we observe, as expected, that the steady-state is reached in a typical time of $\kappa_d/\mathcal{G}^2$ that decreases with g_- [rectangles in Fig. 4(a)]. As a consequence, the stabilization time increases with squeezing when considering a fixed g_+ value, as long as $\mathcal{G}$ dominates both the cavity loss rate κ_c and its self-Kerr rate K. This is well understood from the cooling dynamics of the Bogoliubov mode: larger squeezing parameters $r = \tanh^{-1}(g_+/g_-)$ are obtained for smaller values of $\mathcal{G} = \sqrt{g_-^2 - g_+^2}$ but they lead to a longer stabilization time. The evolution of the squeezing factors

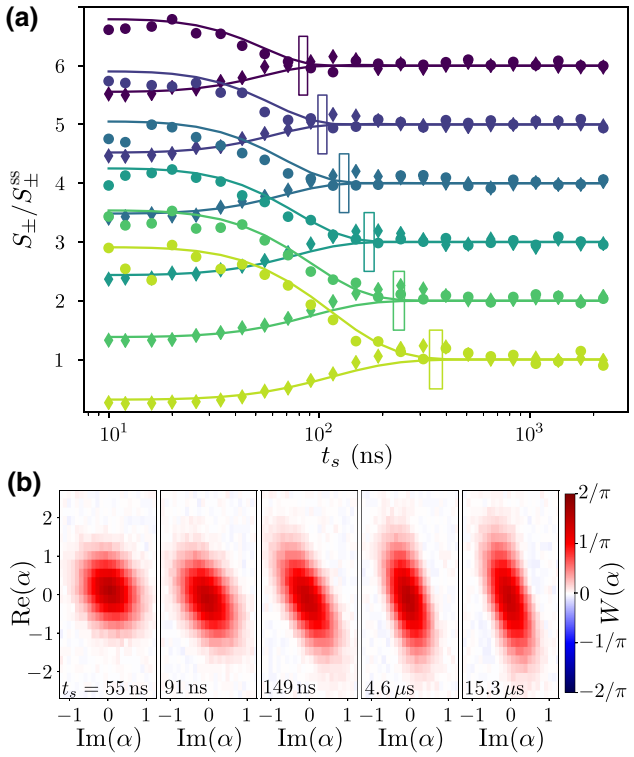

FIG. 4. Dynamics of the squeezing factors. (a) Measured squeezing (dots) and antisqueezing (diamonds) factors normalized by their steady-state values $S_\pm^{\rm ss}$ as a function of the stabilization time t_s for $g_+/2\pi = 1.16$ MHz and various g_-. The data are shifted by 1 for each value of g_- ranging in $g_-/2\pi = [1.48, 1.85, 2.22, 2.59, 2.96, 3.33]$ MHz (from light green to dark blue). Solid lines: results of the numerical simulation. Rectangles indicate the predicted characteristic stabilization times $\kappa_d/\mathcal{G}^2$ assuming 2% relative uncertainty on g_+ and g_-. (b) Selected measured Wigner tomograms for $g_-/2\pi = 1.85$ MHz and $g_+/2\pi = 1.16$ MHz after various stabilization times t_s.

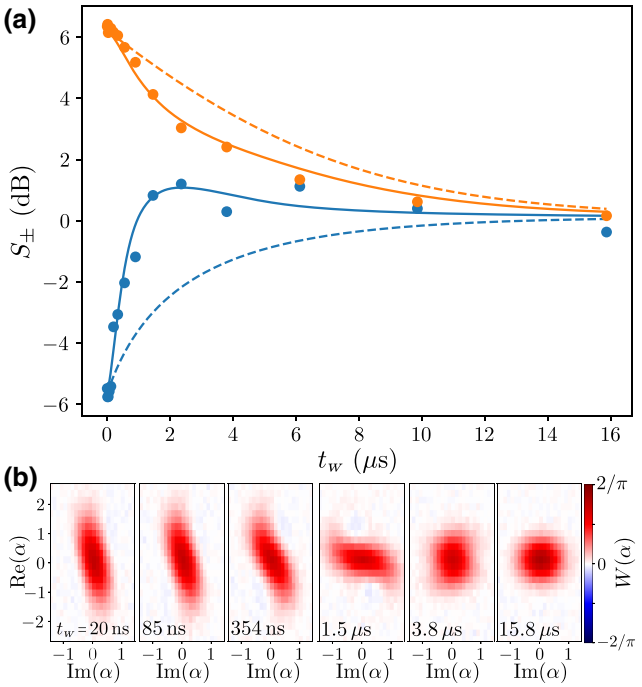

FIG. 5. Decay of the squeezed state towards thermal equilibrium. (a) Dots: measured squeezing factor S_- (blue) and antisqueezing factor S_+ (orange) as a function of the waiting time t_w during which the pumps are turned off after they are at $g_+/2\pi = 1.42$ MHz and $g_-/2\pi = 2.6$ MHz. Solid lines: numerical simulations using $K/\kappa_c = 0.5$. Dashed lines: same simulations but without self-Kerr ($K = 0$). (b) Measured Wigner functions after various pump off times t_w from 20 ns to 15.8 μs as indicated on each label.

is reproduced using numerical simulation of the master equation [solid lines in Fig. 4(a)].

It is also interesting to examine experimentally the time evolution of the full cavity Wigner functions. In Fig. 4(b), the evolution at $g_+/2\pi = 1.16$ MHz and $g_-/2\pi = 1.85$ MHz (global minimum of the squeezing factor) shows how the squeezing establishes with some rotation and distortion of the Gaussian distribution due to Kerr effect as the average number of photons gets larger.

The steady state is thus reached in about $\kappa_d/\mathcal{G}^2$ but how fast does it disappear once the pumps are turned off? Operating at $g_+/2\pi = 1.42$ MHz and $g_-/2\pi = 2.6$ MHz, we perform a Wigner tomography and compute the squeezing and antisqueezing after a waiting time t_w [Fig. 5(a)]. A fast decrease of the squeezing factor is observed in a characteristic time shorter than the cavity relaxation time κ_c^{-1}. We attribute this deviation from the behavior expected of a perfectly harmonic oscillator (dashed lines) to the self-Kerr effect induced by the transmon qubit onto the cavity. The corresponding predicted evolution of squeezing factors is shown with $K/\kappa_c = 0.5$ as solid lines in Fig. 5(a). In numerical simulations, we observe a transition from over-damped to under-damped oscillations of the squeezing factor S_- as K/κ_c increases beyond about 1 (Appendix D 3). Since $K \simeq \kappa_c$ in the experiment, we are close to a critical damping regime.

VI. CONCLUSION

Using dissipation engineering, we show the stabilization of a squeezed state in a microwave resonator with a squeezing factor greatly exceeding the standard 3-dB limit for coherent *in situ* parametric pumping. We directly measure the squeezing factor by performing a direct Wigner tomography using an ancillary qubit. Correcting for state evolution during measurement, we infer that we achieve a squeezing factor of -8.2 ± 0.8 dB. While reservoir-engineered squeezing of mechanical modes has previously been demonstrated, this is the first demonstration of this method (to our knowledge) in an electromagnetic system. The reservoir-engineering technique used here thus extends the state of the art for intraresonator microwave squeezing. Moreover, the produced squeezed state is close to a pure state with purity of 0.91 ± 0.09. A displaced vacuum squeezed state could also be stabilized in our system by adding a coherent drive on the dump.

Beyond the stabilization of Gaussian squeezed states, the techniques presented here could be useful for the stabilization of far more complex states. As discussed, Kerr nonlinearities already play an appreciable role in our experiment. Future work could use this nonlinearity directly as a resource for non-Gaussian state preparation. Recent work has demonstrated that the combination of squeezing-via-parametric driving with Kerr interactions can be used to generate cat states [26,52] and even entangled cat states [53]. The combination of dissipative squeezing (as realized here) with Kerr interactions could similarly yield complex catlike states. Our techniques could also be used to generate squeezed Fock states [68], squeezed Schrödinger's cat states [69], or for the preparation of grid states without the need for measurement [28–31]. These engineered squeezed states could find many applications. Indeed, used to erase which-path information, they can increase gate fidelity [70]; used to increase distinguishability, they can improve qubit-state readout [14,20,71,72]. Squeezing can also be used in spin detection to enhance the light-matter coupling [73,74]. Finally, dissipative squeezing techniques employed on a single site of a lattice of microwave resonators (see, e.g., Ref. [75]) can serve as a shortcut for effectively generating highly entangled many-body states [76,77].

ACKNOWLEDGMENTS

We are grateful to Olivier Arcizet and Alexandre Blais for discussions. This work was initiated during a discussion that happened during Les Houches Summer School in July 2019. We acknowledge IARPA and Lincoln Labs for providing a Josephson Traveling-Wave Parametric Amplifier. The device was fabricated in the cleanrooms of Collège de France, ENS Paris, CEA Saclay, and Observatoire de Paris. This work is part of a project that has received funding from the European Union's Horizon 2020 research and innovation program under Grant Agreement No. 820505. A.C. acknowledges support from the Air Force Office of Scientific Research MURI program, under Grant No. FA9550-19-1-0399.

APPENDIX A: STEADY-STATE WIGNER TOMOGRAMS

The Wigner tomograms of all the points of Fig. 2 are available in Ref. [78].

APPENDIX B: SAMPLE AND SETUP

The sample is the same as in Ref. [41] albeit for a different cool down. The measurement setup is also similar with the addition of the pump at the sum frequency (Fig. 6). The two local oscillators for the pumps are generated by mixing the output of the two microwave sources that are used to generate the dump and cavity drives. Intermediate frequency (IF) signals—tens of MHz—generated by the Quantum Machines' OPX hardware are up-converted by these local oscillators. Finally, we combine and amplify the two pumps before combining them to the dump port inside of the dilution refrigerator.

To successfully stabilize and measure a squeezed state on a well-defined squeezing axis ($g_\pm$ real), a good phase coherence is required between the pumps and cavity drives. Our setup ensures this condition by deriving the

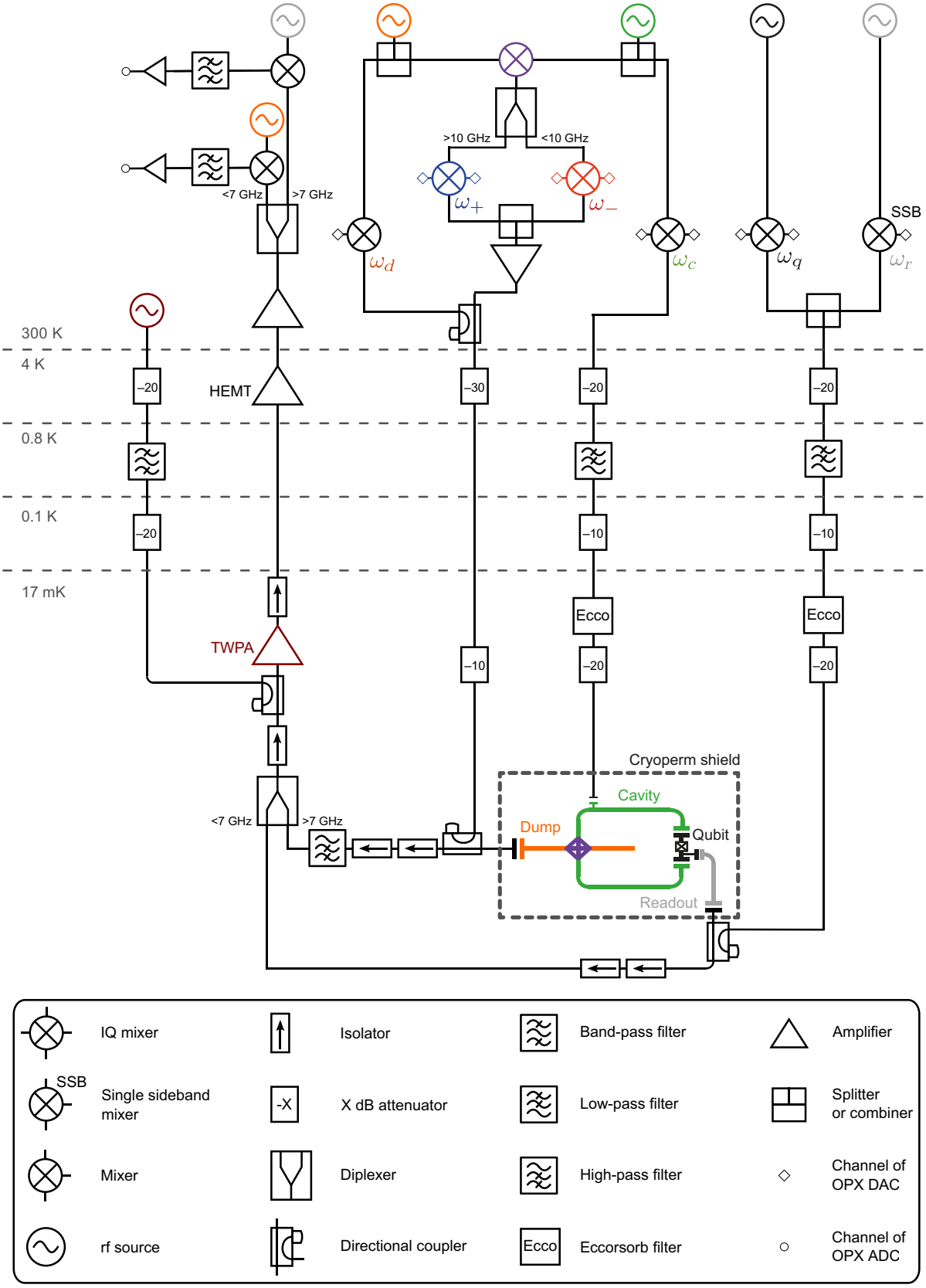

FIG. 6. Schematic of the measurement setup. The color of the rf sources refers to the frequency of the matching element in the device up to a modulation frequency. Multiple instances of a microwave source with the same color represent a single instrument with split outputs. The sum (blue) and difference (red) pumps are obtained by mixing the cavity and dump rf sources to ensure phase stability. The TWPA [79] is provided by Lincoln Labs.

pumps from the dump and cavity local oscillators. One difficulty of our experiment is the large power required for the pumps to reach maximal squeezing factor. This requires the use of a room-temperature amplifier after the mixers (Fig. 6). This amplifier has a slow temperature-induced drift in gain, leading to a relative error of 2% on the pump amplitudes [corresponding to the horizontal errorbars in Fig. 2(b)].

1. Calibration of the pumps

This section shows how to relate the IF amplitudes $\mathcal{A}_-$ and $\mathcal{A}_+$ to the rates g_- and g_+.

To calibrate g_-, we measure the mean photon number in the cavity after applying the pump when the cavity is initially populated with a coherent state $\alpha = \sqrt{6}$. Depending on the amplitude $\mathcal{A}_-$ and duration 4σ of the pump pulse, the rate at which the cavity coherently exchanges excitations with the dump varies (Fig. 7). Due to the large dissipation rate of the dump, the oscillations of the cavity mean photon number $\langle n \rangle$ are damped. By fitting the oscillations using a master equation, we find, as expected, a linear dependence of g_- as a function of $\mathcal{A}_-$ that we use as calibration.

To calibrate g_+, we measure the mean photon number in the cavity n_c^{th} after applying a square pulse with amplitude $\mathcal{A}_+$ for 100 ns when the cavity is initially in vacuum. The mean photon number is measured via cavity-induced Ramsey oscillations [41]. The only difference with the former reference is that the distribution of photon numbers is thermal instead of Poissonian. Hence, the phase acquired by the qubit during the waiting time of the Ramsey sequence

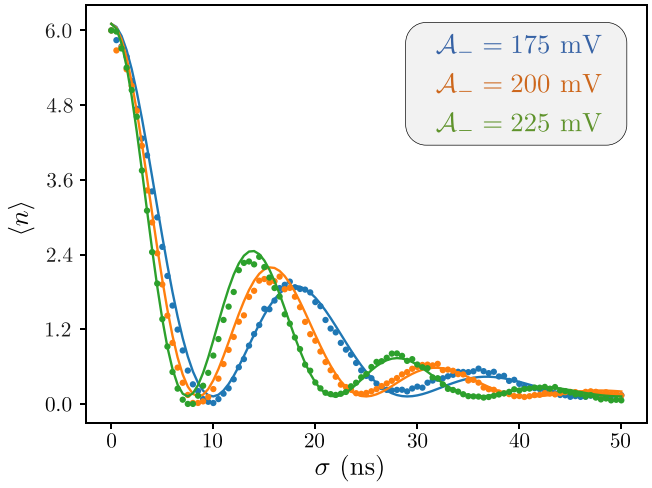

FIG. 7. Calibration of the rate g_-. Dot: measured mean photon number in the cavity as a function of pump-pulse width σ with a hyperbolic secant shape for three amplitudes $\mathcal{A}_-$. Solid lines: prediction of the photon number using a master equation using $g_-/\mathcal{A}_- = 74$ MHz/V.

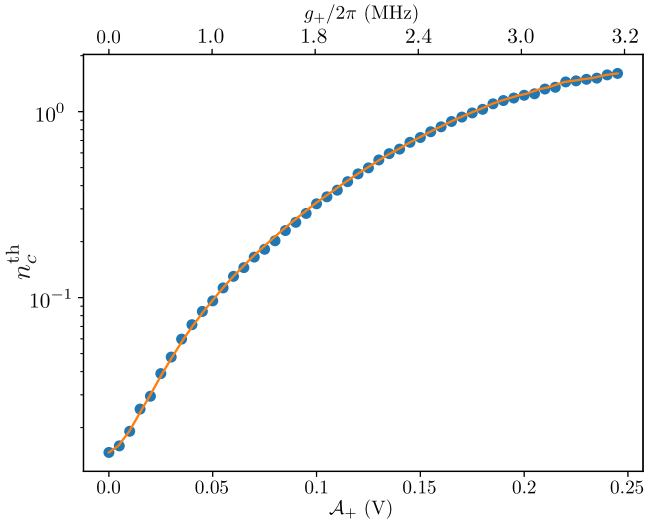

FIG. 8. Calibration of the rate g_+. Dots: measured mean photon number n_c^{th} as a function of the amplitude $\mathcal{A}_+$. Numerical simulations allow us to extract the rate g_+ (top axis) that leads to a given n_c^{th} (see text). Solid line: third-order polynomial fit of g_+ as a function of $\mathcal{A}_+$ that is used as an empirical calibration.

differs and leads to a final qubit excitation probability of

$$P_e(t) = \frac{n_c^{\mathrm{th}}(1-\cos\chi t)+1}{2(1-\cos\chi t)(n_c^{\mathrm{th}}+1)n_c^{\mathrm{th}}+1} e^{-\Gamma_2 t}.$$

Using a time-dependent master equation, the mean photon number is converted into a two-mode squeezing rate g_+. The curve g_+ as a function of $\mathcal{A}_+$ is nonlinear (Fig. 8), likely due to higher-order nonlinearities in the Hamiltonian. The calibration $g_+(\mathcal{A}_+)$ is then obtained by interpolating the measurement.

2. Cavity displacement calibration

The calibration of the displacement of the cavity under a pulsed coherent drive is performed by counting the mean photon number. The method chosen to count the mean photon number is to use the ancillary qubit and readout as a vacuum detector [41]. This method also allows us to extract the cavity decay rate.

3. Cavity thermal population

The cavity thermal population is extracted from the cavity-induced Ramsey oscillations of the ancillary qubit [41]. With the reset protocol, consisting of a swap pulse (g_-) between cavity and dump modes followed by a measurement-based feedback initialization of the qubit in its ground state, we measure a mean photon number $n_c^{\mathrm{th}} = 1.7 \pm 0.3 \times 10^{-2}$ corresponding to an effective temperature of 44 ± 2 mK for the cavity. Note that the swap pulse powers a thermal engine that heats the dump while

cooling down the cavity. The dump here ends up at an effective temperature of at least 144 mK.

4. Correction and uncertainty on the quadrature variances

We wish to extract the squeezing and antisqueezing factors by normalizing the measured variances to the zero-point fluctuations. However, the residual thermal population offsets the measured value of the zero-point fluctuations by a factor $2n_{\mathrm{th}}+1$. This also means that all the measured squeezing factors have to be offset by 0.15 ± 0.03 dB. Due to other sources of uncertainty, such as fluctuations on the cavity-displacement pulses, we measure a higher statistical uncertainty for the pump-off variances of ± 0.2 dB.

APPENDIX C: KERR-FREE ANALYTICAL MODEL

This derivation, which can be found in Ref. [24], is given here for completeness. When continuously pumping at the difference and sum of the resonance frequencies with rates g_- and g_+, the Langevin equations read

$$\begin{aligned}\dot{\hat{d}} &= -\frac{\kappa_d}{2}\hat{d} + i(g_-\hat{c} + g_+\hat{c}^\dagger) + \sqrt{\kappa_d}\hat{d}_{\mathrm{in}},\\ \dot{\hat{c}} &= -\frac{\kappa_c}{2}\hat{c} + i(g_-\hat{d} + g_+\hat{d}^\dagger) + \sqrt{\kappa_c}\hat{c}_{\mathrm{in}},\end{aligned} \tag{C1}$$

where the cavity (dump) input field operators $\hat{c}_{\mathrm{in}}$ ($\hat{d}_{\mathrm{in}}$) verify $[\hat{b}_{\mathrm{in}}(t), \hat{b}_{\mathrm{in}}(t')] = \delta(t-t')$ and $\langle \hat{b}^\dagger_{\mathrm{in}}(t)\hat{b}_{\mathrm{in}}(t')\rangle = n_{\mathrm{b}}^{\mathrm{th}}\delta(t-t')$ for $b = c, d$. Solving the Langevin equations for the steady state, the squeezing S_- and antisqueezing S_+ factors are given by

$$\begin{aligned}S_\pm = &\frac{4(g_- \mp g_+)^2\kappa_d(2n_d^{\mathrm{th}}+1)}{(\kappa_d+\kappa_c)(4\mathcal{G}^2+\kappa_d\kappa_c)}\\ &+\frac{[4\mathcal{G}^2+\kappa_d(\kappa_d+\kappa_c)]\kappa_c(2n_c^{\mathrm{th}}+1)}{(\kappa_d+\kappa_c)(4\mathcal{G}^2+\kappa_d\kappa_c)}.\end{aligned} \tag{C2}$$

Assuming $\mathcal{G}, \kappa_c \ll \kappa_d$, Eq. (C2) gives the simplified Eq. (4) given in the main text.

APPENDIX D: MODELING THE KERR EFFECT

The Kerr effect is not included in the analytical model described in Appendix C. It induces spurious effects, which reduce the maximal squeezing factor and accelerate the relaxation of squeezing. In this section, we show how to take these effects into account. We simulate our system using the QuantumOptics.jl library [80]. The steady-state simulations are run on an Nvidia Geforce 1080Ti GPU, which allows us to reach Hilbert space dimensions of about 1800. All of the other simulations are run on the CPU. Except for the Wigner-tomography retroprediction, the qubit is not simulated but we take into account the Kerr effect it induces on the cavity. In the case of the Wigner-tomography retroprediction, the dump is adiabatically eliminated.

1. Retroprediction of the Wigner tomography

In order to correct for the error introduced by the cavity evolution during Wigner tomography, we resort to simulations of the cavity and qubit alone. Indeed, in the absence of pumps, the effect of the JRM on the cavity is negligible. We numerically implement our experimental Wigner-tomography pulse sequence on a truncated Hilbert with up to 50 excitations for the cavity and the two qubit states. Starting from a range of initial squeezed states for the cavity, with variances (S^i_-, S^i_+), we simulate the outcome of the faulty Wigner tomography by computing the variances (S^W_-, S^W_+) of the simulated Wigner tomograms.

This dataset provides a function f_W that maps actual variances (S^i_-, S^i_+) of the premeasured quantum state to the variances (S^W_-, S^W_+) extracted from the measured Wigner tomograms. As this function empirically appears bijective, the retroprediction is performed by interpolating its inverse f_W^{-1}. The interpolated f_W^{-1} for the initial squeezing and antisqueezing, as well as the simulated points, are shown in Figs. 9(a) and 9(b), respectively. The retropredicted initial squeezing and antisqueezing corresponding to Figs. 2(a) and 2(b) are shown in Figs. 9(c) and 9(d), respectively.

Assuming the ± 0.2 dB of uncertainty on the measured $S^W_\pm$, and retropredicting the evolution during Wigner tomography, we obtain an uncertainty $\Delta S_\pm$ on the retropredicted squeezing and antisqueezing factors that depends on the value of the measured squeezing and antisqueezing [Figs. 9(e) and 9(f)].

2. Steady-state simulations

As seen in Fig. 2(b), the analytical Kerr-free model fails to quantitatively describe the squeezing factor at $g_+ > 0.7g_-$ [Fig. 10(a)]. Here, we compute how higher-order terms in the Hamiltonian may explain this difference. The first term we consider is the Kerr effect $-Kc^{\dagger 2}c^2$ induced by the qubit on the cavity [Fig. 10(b)]. This simulation accurately predicts the optimal g_+ but still fails to reproduce the measured squeezing factors above $g_+/g_- = 0.7$. Experimentally, we aim for a JRM flux bias that maximizes the three-wave mixing term while canceling the four-wave mixing term. However, small deviations from this sweet spot create four-wave mixing terms between the cavity, dump, and pumps. Contrary to the retroprediction simulations, which model a situation where the pumps are turned off, these extra terms may have a significant impact on the squeezing factor where the pumps are turned on. In the RWA, the four-wave mixing term leads to three kinds of interactions, a cross-Kerr between

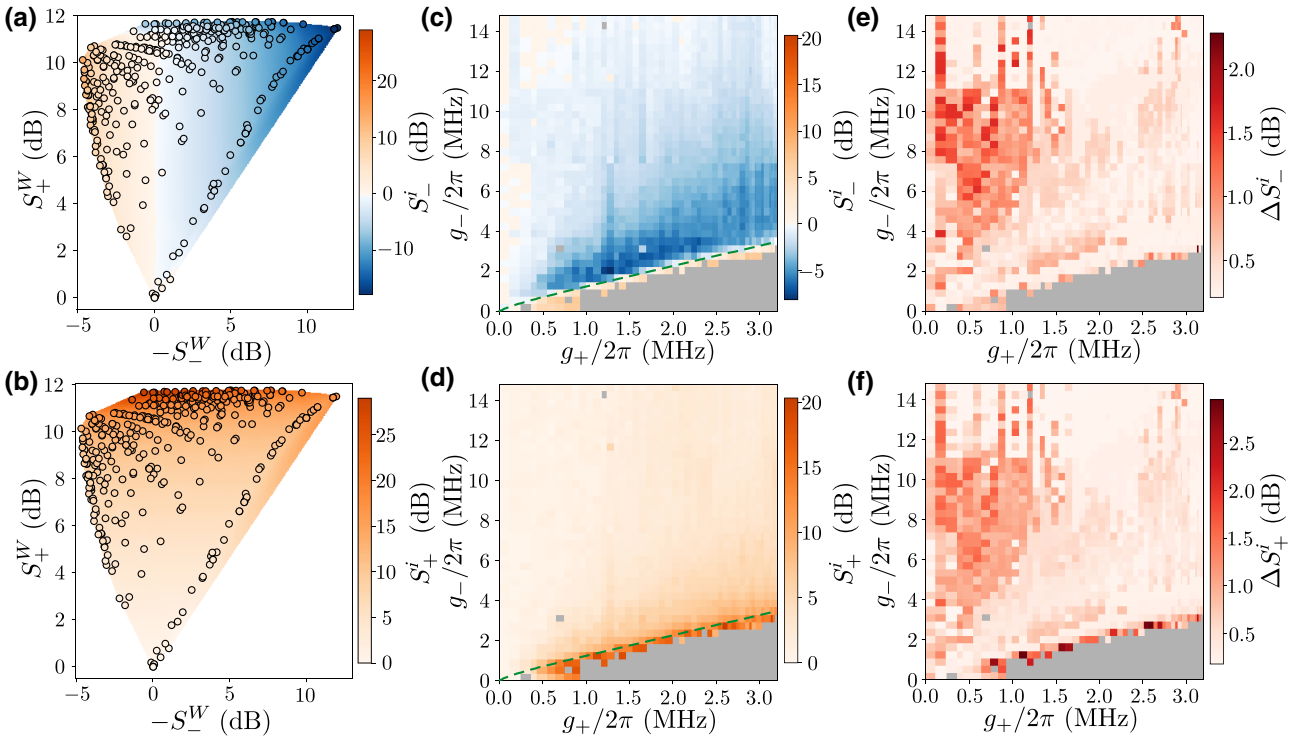

FIG. 9. (a),(b) Representation of the map f_W^{-1}. Premeasurement squeezing S_-^i and antisqueezing S_+^i as a function of the measured squeezing and antisqueezing factors $S_\pm^W$. Circles: simulated values. Colors: linear interpolation of f_W^{-1}. (c),(d) Version of Fig. 2(a) corrected for the measurement error during Wigner tomography. (e),(f) Color: retropredicted uncertainty on the squeezing factors ΔS_-^i and ΔS_+^i owing to a measurement uncertainty of ± 0.2 dB on $S_\pm^W$.

cavity and dump $K_{\rm cd}c^\dagger c d^\dagger d$, an ac Stark frequency shift due to the pumps $2(|p_-|^2+|p_+|^2)(K_{\rm pc}c^\dagger c + K_{\rm pd}d^\dagger d)$ and parametric squeezing drive due to pump intermodulation $K_{\rm pc}p_+p_-^* c^{\dagger 2} + K_{\rm pd}p_+^* p_-^* d^{\dagger 2}$ + h.c.. The JRM also induces a self-Kerr interaction for the dump, but we neglect it as it is one order of magnitude smaller than $K_{\rm pd}p_+^*p_-^*$ in our case [81] and much smaller than the dissipation rate κ_d anyway. The rates $K_{\rm cd}$, $K_{\rm pc}$, and $K_{\rm pd}$ ('cd', 'pc' and 'pd' denote 'cavity dump', 'pump cavity', and 'pump dump' respectively) are not measured in this run. Realistic values $K_{\rm cd}/2\pi = 250$ kHz, $K_{\rm pc}|p_-|^2/2\pi = 172$ kHz, and $K_{\rm pd}|p_-|^2/2\pi = 172$ kHz can change the squeezing factors at the large g_+, which comforts the assumption that higher-order nonlinearities may explain the deviations we observe between our analytical model and the measured squeezing factors.

To numerically compute the steady-state squeezing and antisqueezing as a function of g_- and g_+, we use an

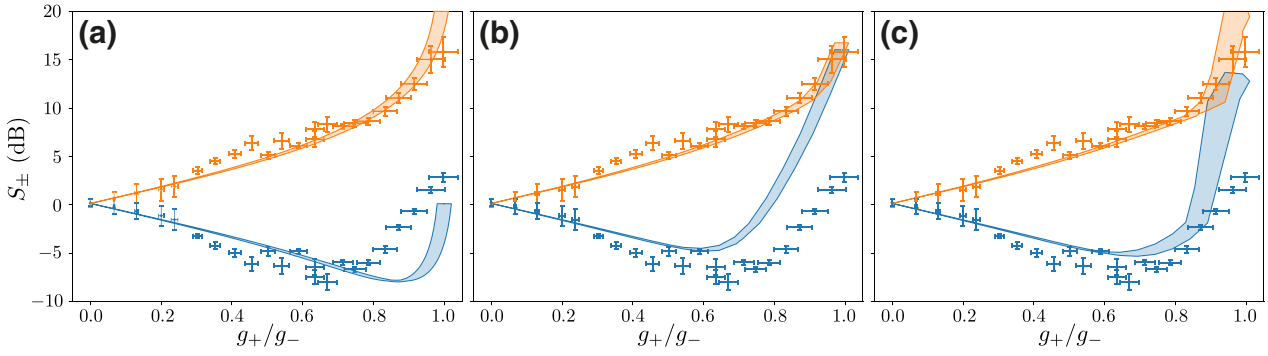

FIG. 10. (a)–(c) Crosses, retropredicted squeezing factors for $g_-/2\pi = 1.85$ MHz as in Fig. 2(b). Shaded areas correspond to different models with 2% uncertainty on g_+ and g_-; in (a), Kerr-free analytical model, in (b), steady-state simulations with $K/2\pi = 20 \pm 2$ kHz, in (c), steady-state simulations, including, in addition to the Kerr effect, some JRM four-wave mixing terms, $K_{\rm cd}/2\pi = 250$ kHz, $K_{\rm pc}|p_-|^2/2\pi = 172 \pm 4$ kHz, and $K_{\rm pd}|p_-|^2/2\pi = 172 \pm 4$ kHz.

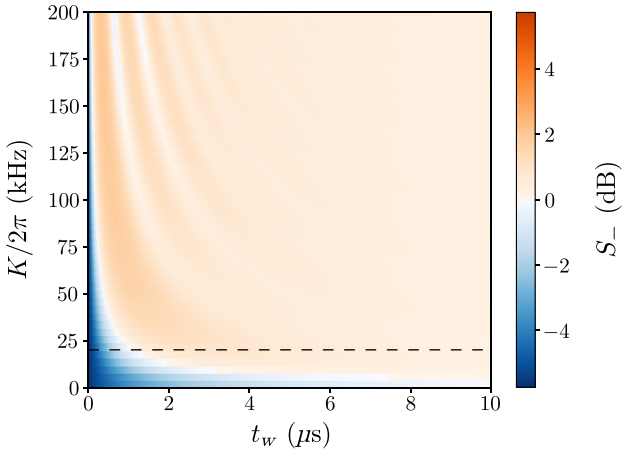

FIG. 11. Color: simulated squeezing factor S_- as a function of waiting time t_w and cavity self-Kerr rate K for an initial state with squeezing factor $S_- = -5.7$ dB and antisqueezing of $S_+ = 6.2$ dB. The dashed line indicates our device parameter $K/2\pi = 20$ kHz.

iterative method to find the Liouvillian eigenvalues on a truncated Hilbert space comprising up to 60 excitations for the cavity and 30 excitations for the dump.

3. Simulations of the squeezing dynamics

The dynamics of stabilization and decay of squeezing are computed by solving the master equation on a truncated Hilbert space comprising up to 20 excitations for the cavity and 16 excitations for the dump.

To understand the effect of the self-Kerr term on the squeezing decay, we simulate the evolution of squeezing for varying waiting time t_w and various self-Kerr rates K (Fig. 11). We initialize the cavity state at $t_w = 0$ in a Gaussian state with the measured $S_- = -5.7$ dB and $S_+ = 6.2$ dB of Fig. 5(a). Dismissing the Kerr effect ($K = 0$), we observe an exponential damping of squeezing due to the cavity relaxation. For nonzero K, the squeezing factor also oscillates in time. Our experimental value $K/2\pi = 20$ kHz is closed to the critically damped regime where the effective decay time is maximally reduced. This observation highlights the crucial role of Kerr effect in the imperfections of our Wigner-tomography technique used to estimate the variances.

APPENDIX E: EFFECT OF FINITE-SIZE WIGNER TOMOGRAMS

Due to experimental constraints, the probed quadrature phase space must be finite. A rectangular window $-x_0 \leq \mathrm{Im}(\alpha) \leq x_0$ and $-y_0 \leq \mathrm{Re}(\alpha) \leq y_0$ is chosen, where $x_0 = 1.4$ and $y_0 = 2.7$. This induces a systematic error on the estimation of the variances. Indeed, the variances $\langle X_-^2 \rangle$ and $\langle X_+^2 \rangle$ are computed from the Wigner function using $\langle X_-^2 \rangle = \min_\theta \int_{-\infty}^{\infty} \mathrm{Im}(\alpha e^{i\theta})^2 W(\alpha) d^2\alpha$ and $\langle X_+^2 \rangle = \max_\theta \int_{-\infty}^{\infty} \mathrm{Re}(\alpha e^{i\theta})^2 W(\alpha) d^2\alpha$. Assuming a vacuum squeezed state with minimal variance $\langle X_-^2 \rangle = \sigma^2$ and maximal variance $\langle X_+^2 \rangle = 1/\sigma^2$, its Wigner function is given by

$$W(\alpha) = \frac{2}{\pi} \exp\left[-\mathrm{Re}(\alpha e^{i\theta_{\min}})^2 \sigma^2 - \mathrm{Im}(\alpha e^{i\theta_{\min}})^2 / \sigma^2\right].$$

Knowing only the Wigner function in a window $[-y_0, y_0]$ over the real axis, the inferred maximum variance is

$$\langle X_{+_{y_0}}^2 \rangle = \left[-2\sigma y_0 e^{-y_0^2\sigma^2}/\sqrt{\pi} + \mathrm{Erf}(y_0\sigma)\right] \frac{1}{\sigma^2}.$$

This variance saturates as a function of σ towards a value of 11 dB in our case. This means that we are unable to resolve any variance above 11 dB along the real axis.

[1] H. J. Kimble, Y. Levin, A. B. Matsko, K. S. Thorne, and S. P. Vyatchanin, Conversion of conventional gravitational-wave interferometers into quantum nondemolition interferometers by modifying their input and/or output optics, Phys. Rev. D **65**, 022002 (2001).

[2] J. Abadie, *et al.*, A gravitational wave observatory operating beyond the quantum shot-noise limit, Nat. Phys. **7**, 962 (2011).

[3] J. Aasi, *et al.*, Enhanced sensitivity of the ligo gravitational wave detector by using squeezed states of light, Nat. Photonics **7**, 613 (2013).

[4] M. Korobko, L. Kleybolte, S. Ast, H. Miao, Y. Chen, and R. Schnabel, Beating the Standard Sensitivity-Bandwidth Limit of Cavity-Enhanced Interferometers with Internal Squeezed-Light Generation, Phys. Rev. Lett. **118**, 143601 (2017).

[5] Drummond and Ficek, *Quantum Squeezing* (Springer Science & Business Media, New York, 2013).

[6] S. L. Braunstein and P. van Loock, Quantum information with continuous variables, Rev. Mod. Phys. **77**, 513 (2005).

[7] H.-S. Zhong, H. Wang, Y.-H. Deng, M.-C. Chen, L.-C. Peng, Y.-H. Luo, J. Qin, D. Wu, X. Ding, Y. Hu, P. Hu, X.-Y. Yang, W.-J. Zhang, H. Li, Y. Li, X. Jiang, L. Gan, G. Yang, L. You, Z. Wang, L. Li, N.-L. Liu, C.-Y. Lu, and J.-W. Pan, Quantum computational advantage using photons, Science **370**, 1460 (2020).

[8] C. W. Gardiner and M. J. Collett, Input and output in damped quantum systems: Quantum stochastic differential equations and the master equation, Phys. Rev. A **31**, 3761 (1985).

[9] G. Milburn and D. Walls, Production of squeezed states in a degenerate parametric amplifier, Opt. Commun. **39**, 401 (1981).

[10] M. J. Collett and C. W. Gardiner, Squeezing of intracavity and traveling-wave light fields produced in parametric amplification, Phys. Rev. A **30**, 1386 (1984).

[11] J. B. Clark, F. Lecocq, R. W. Simmonds, J. Aumentado, and J. D. Teufel, Sideband cooling beyond the quantum backaction limit with squeezed light, Nature **541**, 191 (2017).

[12] A. Bienfait, P. Campagne-Ibarcq, A. H. Kiilerich, X. Zhou, S. Probst, J. J. Pla, T. Schenkel, D. Vion, D. Esteve, J. J. L. Morton, K. Moelmer, and P. Bertet, Magnetic Resonance with Squeezed Microwaves, Phys. Rev. X **7**, 041011 (2017).

[13] S. Kono, Y. Masuyama, T. Ishikawa, Y. Tabuchi, R. Yamazaki, K. Usami, K. Koshino, and Y. Nakamura, Nonclassical Photon Number Distribution in a Superconducting Cavity Under a Squeezed Drive, Phys. Rev. Lett. **119**, 023602 (2017).

[14] A. Eddins, S. Schreppler, D. M. Toyli, L. S. Martin, S. Hacohen-Gourgy, L. C. G. Govia, H. Ribeiro, A. A. Clerk, and I. Siddiqi, Stroboscopic Qubit Measurement with Squeezed Illumination, Phys. Rev. Lett. **120**, 040505 (2018).

[15] M. Malnou, D. A. Palken, B. M. Brubaker, L. R. Vale, G. C. Hilton, and K. W. Lehnert, Squeezed Vacuum Used to Accelerate the Search for a Weak Classical Signal, Phys. Rev. X **9**, 021023 (2019).

[16] K. M. Backes, *et al.*, A quantum enhanced search for dark matter axions, Nature **590**, 238 (2021).

[17] J. F. Poyatos, J. I. Cirac, and P. Zoller, Quantum Reservoir Engineering with Laser Cooled Trapped Ions, Phys. Rev. Lett. **77**, 4728 (1996).

[18] J. I. Cirac, A. S. Parkins, R. Blatt, and P. Zoller, "Dark" Squeezed States of the Motion of a Trapped Ion, Phys. Rev. Lett. **70**, 556 (1993).

[19] A. Kronwald, F. Marquardt, and A. A. Clerk, Arbitrarily large steady-state bosonic squeezing via dissipation, Phys. Rev. A **88**, 1 (2013).

[20] N. Didier, F. Qassemi, and A. Blais, Perfect squeezing by damping modulation in circuit quantum electrodynamics, Phys. Rev. A **89**, 013820 (2014).

[21] E. E. Wollman, C. U. Lei, A. J. Weinstein, J. Suh, A. Kronwald, F. Marquardt, A. A. Clerk, and K. C. Schwab, Quantum squeezing of motion in a mechanical resonator, Science **349**, 952 (2015).

[22] J.-M. Pirkkalainen, E. Damskägg, M. Brandt, F. Massel, and M. A. Sillanpää, Squeezing of Quantum Noise of Motion in a Micromechanical Resonator, Phys. Rev. Lett. **115**, 243601 (2015).

[23] F. Lecocq, J. B. Clark, R. W. Simmonds, J. Aumentado, and J. D. Teufel, Quantum Nondemolition Measurement of A Nonclassical State of a Massive Object, Phys. Rev. X **5**, 041037 (2015).

[24] C. U. Lei, A. J. Weinstein, J. Suh, E. E. Wollman, A. Kronwald, F. Marquardt, A. A. Clerk, and K. C. Schwab, Quantum Nondemolition Measurement of a Quantum Squeezed State Beyond the 3 dB Limit, Phys. Rev. Lett. **117**, 100801 (2016).

[25] D. Kienzler, H.-Y. Lo, B. Keitch, L. de Clercq, F. Leupold, F. Lindenfelser, M. Marinelli, V. Negnevitsky, and J. P. Home, Quantum harmonic oscillator state synthesis by reservoir engineering, Science **347**, 53 (2015).

[26] S. Puri, S. Boutin, and A. Blais, Engineering the quantum states of light in a Kerr-nonlinear resonator by two-photon driving, npj Quantum Inf. **3**, 18 (2017).

[27] A. Grimm, N. E. Frattini, S. Puri, S. O. Mundhada, S. Touzard, M. Mirrahimi, S. M. Girvin, S. Shankar, and M. H. Devoret, Stabilization and operation of a Kerr-cat qubit, Nature **584**, 205 (2020).

[28] P. Campagne-Ibarcq, A. Eickbusch, S. Touzard, E. Zalys-Geller, N. E. Frattini, V. V. Sivak, P. Reinhold, S. Puri, S. Shankar, R. J. Schoelkopf, L. Frunzio, M. Mirrahimi, and M. H. Devoret, Quantum error correction of a qubit encoded in grid states of an oscillator, Nature **584**, 368 (2020).

[29] C. Flühmann, T. L. Nguyen, M. Marinelli, V. Negnevitsky, K. Mehta, and J. P. Home, Encoding a qubit in a trapped-ion mechanical oscillator, Nature **566**, 513 (2019).

[30] J. Hastrup, K. Park, J. B. Brask, R. Filip, and U. L. Andersen, Measurement-free preparation of grid states, npj Quantum Inf. **7**, 17 (2021).

[31] B. D. Neeve, T. Behrle, and J. P. Home, arXiv:2010.09681v1 (2020).

[32] L. G. Lutterbach and L. Davidovich, Method for Direct Measurement of the Wigner Function in Cavity QED and Ion Traps, Phys. Rev. Lett. **78**, 2547 (1997).

[33] P. Bertet, A. Auffeves, P. Maioli, S. Osnaghi, T. Meunier, M. Brune, J. M. Raimond, and S. Haroche, Direct Measurement of the Wigner Function of a One-Photon Fock State in a Cavity, Phys. Rev. Lett. **89**, 200402 (2002).

[34] B. Vlastakis, G. Kirchmair, Z. Leghtas, S. E. Nigg, L. Frunzio, S. M. Girvin, M. Mirrahimi, M. H. Devoret, and R. J. Schoelkopf, Deterministically encoding quantum information using 100-photon Schrödinger cat states, Science **342**, 607 (2013).

[35] N. Bergeal, F. Schackert, M. Metcalfe, R. Vijay, V. E. Manucharyan, L. Frunzio, D. E. Prober, R. J. Schoelkopf, S. M. Girvin, and M. H. Devoret, Phase-preserving amplification near the quantum limit with a Josephson ring modulator, Nature **465**, 64 (2010).

[36] N. Bergeal, R. Vijay, V. E. Manucharyan, I. Siddiqi, R. J. Schoelkopf, S. M. Girvin, and M. H. Devoret, Analog information processing at the quantum limit with a Josephson ring modulator, Nat. Phys. **6**, 296 (2010).

[37] B. Abdo, K. Sliwa, F. Schackert, N. Bergeal, M. Hatridge, L. Frunzio, A. D. Stone, and M. Devoret, Full Coherent Frequency Conversion between Two Propagating Microwave Modes, Phys. Rev. Lett. **110**, 173902 (2013).

[38] N. Roch, E. Flurin, F. Nguyen, P. Morfin, P. Campagne-Ibarcq, M. H. Devoret, and B. Huard, Widely Tunable, Nondegenerate Three-Wave Mixing Microwave Device Operating near the Quantum Limit, Phys. Rev. Lett. **108**, 147701 (2012).

[39] E. Flurin, N. Roch, F. Mallet, M. H. Devoret, and B. Huard, Generating Entangled Microwave Radiation Over Two Transmission Lines, Phys. Rev. Lett. **109**, 1 (2012).

[40] T. Peronnin, D. Marković, Q. Ficheux, and B. Huard, Sequential Dispersive Measurement of a Superconducting Qubit, Phys. Rev. Lett. **124**, 180502 (2020).

[41] R. Dassonneville, R. Assouly, T. Peronnin, P. Rouchon, and B. Huard, Number-Resolved Photocounter for Propagating Microwave Mode, Phys. Rev. Appl. **14**, 044022 (2020).

[42] S. Fedortchenko, S. Felicetti, D. Marković, S. Jezouin, A. Keller, T. Coudreau, B. Huard, and P. Milman, Quantum simulation of ultrastrongly coupled bosonic modes using superconducting circuits, Phys. Rev. A **95**, 042313 (2017).

[43] D. Marković, S. Jezouin, Q. Ficheux, S. Fedortchenko, S. Felicetti, T. Coudreau, P. Milman, Z. Leghtas, and B. Huard, Demonstration of an Effective Ultrastrong Coupling between Two Oscillators, Phys. Rev. Lett. **121**, 040505 (2018).

[44] D. Marković, J. Pillet, E. Flurin, N. Roch, and B. Huard, Injection Locking and Parametric Locking in a Superconducting Circuit, Phys. Rev. Appl. **12**, 024034 (2019).

[45] A. Metelmann and A. A. Clerk, Nonreciprocal quantum interactions and devices via autonomous feedforward, Phys. Rev. A **95**, 013837 (2017).

[46] A. Metelmann and A. A. Clerk, Nonreciprocal Photon Transmission and Amplification via Reservoir Engineering, Phys. Rev. X **5**, 021025 (2015).

[47] T.-C. Chien, O. Lanes, C. Liu, X. Cao, P. Lu, S. Motz, G. Liu, D. Pekker, and M. Hatridge, Multiparametric amplification and qubit measurement with a Kerr-free Josephson ring modulator, Phys. Rev. A **101**, 042336 (2020).

[48] L. Zhong, E. P. Menzel, R. D. Candia, P. Eder, M. Ihmig, A. Baust, M. Haeberlein, E. Hoffmann, K. Inomata, T. Yamamoto, Y. Nakamura, E. Solano, F. Deppe, A. Marx, and R. Gross, Squeezing with a flux-driven josephson parametric amplifier, New J. Phys. **15**, 125013 (2013).

[49] A. Kronwald, F. Marquardt, and A. A. Clerk, Dissipative optomechanical squeezing of light, New J. Phys. **16**, 063058 (2014).

[50] C. F. Ockeloen-Korppi, E. Damskägg, J.-M. Pirkkalainen, T. T. Heikkilä, F. Massel, and M. A. Sillanpää, Noiseless Quantum Measurement and Squeezing of Microwave Fields Utilizing Mechanical Vibrations, Phys. Rev. Lett. **118**, 103601 (2017).

[51] S. Boutin, D. M. Toyli, A. V. Venkatramani, A. W. Eddins, I. Siddiqi, and A. Blais, Effect of Higher-Order Nonlinearities on Amplification and Squeezing in Josephson Parametric Amplifiers, Phys. Rev. Appl. **8**, 054030 (2017).

[52] H. Goto, Bifurcation-based adiabatic quantum computation with a nonlinear oscillator network, Sci. Rep. **6**, 21686 (2016).

[53] M. Mamaev, L. C. G. Govia, and A. A. Clerk, Dissipative stabilization of entangled cat states using a driven Bose-Hubbard dimer, Quantum **2**, 58 (2018).

[54] G. Kirchmair, B. Vlastakis, Z. Leghtas, S. E. Nigg, H. Paik, E. Ginossar, M. Mirrahimi, L. Frunzio, S. M. Girvin, and R. J. Schoelkopf, Observation of quantum state collapse and revival due to the single-photon Kerr effect, Nature **495**, 205 (2013).

[55] R. Lescanne, L. Verney, Q. Ficheux, M. H. Devoret, B. Huard, M. Mirrahimi, and Z. Leghtas, Escape of a Driven Quantum Josephson Circuit Into Unconfined States, Phys. Rev. Appl. **11**, 14030 (2019).

[56] P. Six, P. Campagne-Ibarcq, I. Dotsenko, A. Sarlette, B. Huard, and P. Rouchon, Quantum state tomography with noninstantaneous measurements, imperfections, and decoherence, Phys. Rev. A **93**, 12109 (2016).

[57] M. Malnou, D. A. Palken, L. R. Vale, G. C. Hilton, and K. W. Lehnert, Optimal Operation of a Josephson Parametric Amplifier for Vacuum Squeezing, Phys. Rev. Appl. **9**, 044023 (2018).

[58] F. Mallet, M. A. Castellanos-Beltran, H. S. Ku, S. Glancy, E. Knill, K. D. Irwin, G. C. Hilton, L. R. Vale, and K. W. Lehnert, Quantum State Tomography of an Itinerant Squeezed Microwave Field, Phys. Rev. Lett. **106**, 220502 (2011).

[59] S. Pogorzalek, K. G. Fedorov, M. Xu, A. Parra-Rodriguez, M. Sanz, M. Fischer, E. Xie, K. Inomata, Y. Nakamura, E. Solano, A. Marx, F. Deppe, and R. Gross, Secure quantum remote state preparation of squeezed microwave states, Nat. Commun. **10**, 2604 (2019).

[60] R. W. Heeres, B. Vlastakis, E. Holland, S. Krastanov, V. V. Albert, L. Frunzio, L. Jiang, and R. J. Schoelkopf, Cavity State Manipulation Using Photon-Number Selective Phase Gates, Phys. Rev. Lett. **115**, 1 (2015).

[61] W. Wang, L. Hu, Y. Xu, K. Liu, Y. Ma, S.-B. Zheng, R. Vijay, Y. P. Song, L.-M. Duan, and L. Sun, Converting Quasiclassical States Into Arbitrary Fock State Superpositions in a Superconducting Circuit, Phys. Rev. Lett. **118**, 223604 (2017).

[62] D. M. Meekhof, C. Monroe, B. E. King, W. M. Itano, and D. J. Wineland, Generation of Nonclassical Motional States of a Trapped Atom, Phys. Rev. Lett. **76**, 1796 (1996).

[63] S. C. Burd, R. Srinivas, J. J. Bollinger, A. C. Wilson, D. J. Wineland, D. Leibfried, D. H. Slichter, and D. T. C. Allcock, Quantum amplification of mechanical oscillator motion, Science **364**, 1163 (2019).

[64] D. I. Schuster, A. A. Houck, J. A. Schreier, A. Wallraff, J. M. Gambetta, A. Blais, L. Frunzio, J. Majer, B. Johnson, M. H. Devoret, S. M. Girvin, and R. J. Schoelkopf, Resolving photon number states in a superconducting circuit, Nature **445**, 515 (2007).

[65] E. Flurin, N. Roch, J. D. Pillet, F. Mallet, and B. Huard, Superconducting Quantum Node for Entanglement and Storage of Microwave Radiation, Phys. Rev. Lett. **114**, 90503 (2015).

[66] D. N. Klyshko, Observable signs of nonclassical light, Phys. Lett. A **213**, 7 (1996).

[67] V. V. Dodonov, 'Nonclassical' states in quantum optics: A 'squeezed' review of the first 75 years, J. Opt. B: Quantum Semiclassical Opt. **4**, R1 (2002).

[68] D. Kienzler, H.-Y. Lo, V. Negnevitsky, C. Flühmann, M. Marinelli, and J. P. Home, Quantum Harmonic Oscillator State Control in a Squeezed Fock Basis, Phys. Rev. Lett. **119**, 033602 (2017).

[69] H.-Y. Lo, D. Kienzler, L. de Clercq, M. Marinelli, V. Negnevitsky, B. C. Keitch, and J. P. Home, Spin–motion entanglement and state diagnosis with squeezed oscillator wavepackets, Nature **521**, 336 (2015).

[70] S. Puri and A. Blais, High-Fidelity Resonator-Induced Phase Gate with Single-Mode Squeezing, Phys. Rev. Lett. **116**, 180501 (2016).

[71] N. Didier, J. Bourassa, and A. Blais, Fast Quantum Nondemolition Readout by Parametric Modulation of Longitudinal Qubit-Oscillator Interaction, Phys. Rev. Lett. **115**, 203601 (2015).

[72] S. Touzard, A. Kou, N. E. Frattini, V. V. Sivak, S. Puri, A. Grimm, L. Frunzio, S. Shankar, and M. H. Devoret, Gated Conditional Displacement Readout of Superconducting Qubits, Phys. Rev. Lett. **122**, 80502 (2019).

[73] C. Leroux, L. C. G. Govia, and A. A. Clerk, Enhancing Cavity Quantum Electrodynamics Via Antisqueezing: Synthetic Ultrastrong Coupling, Phys. Rev. Lett. **120**, 093602 (2018).

[74] W. Qin, A. Miranowicz, P.-B. Li, X.-Y. Lü, J. Q. You, and F. Nori, Exponentially Enhanced Light-Matter Interaction,

Cooperativities, and Steady-State Entanglement Using Parametric Amplification, Phys. Rev. Lett. **120**, 093601 (2018).

[75] C. Owens, A. LaChapelle, B. Saxberg, B. M. Anderson, R. Ma, J. Simon, and D. I. Schuster, Quarter-flux Hofstadter lattice in a qubit-compatible microwave cavity array, Phys. Rev. A **97**, 013818 (2018).

[76] Y. Yanay and A. A. Clerk, Reservoir engineering of bosonic lattices using chiral symmetry and localized dissipation, Phys. Rev. A **98**, 043615 (2018).

[77] Y. Yanay and A. A. Clerk, Reservoir engineering with localized dissipation: Dynamics and prethermalization, Phys. Rev. Res. **2**, 023177 (2020).

[78] R. Dassonneville, R. Assouly, T. Peronnin, A. Clerk, A. Bienfait, and B. Huard, Steady-state wigner tomograms, Zenodo (2020), https://zenodo.org/record/4320822.

[79] C. Macklin, K. O'Brien, D. Hover, M. E. Schwartz, V. Bolkhovsky, X. Zhang, W. D. Oliver, and I. Siddiqi, A near–quantum-limited Josephson traveling-wave parametric amplifier, Science **350**, 307 (2015).

[80] S. Krämer, D. Plankensteiner, L. Ostermann, and H. Ritsch, QuantumOptics.jl: A Julia framework for simulating open quantum systems, Comput. Phys. Commun. **227**, 109 (2018).

[81] E. Flurin, Ph.D. thesis, École Normale Supérieure (2014), https://tel.archives-ouvertes.fr/tel-01241123.